

The flux-weighted gravity-luminosity relation of Galactic classical Cepheids [★]

M. A. T. Groenewegen

Koninklijke Sterrenwacht van België, Ringlaan 3, B-1180 Brussels, Belgium
e-mail: martin.groenewegen@oma.be

received: ** 2020, accepted: * 2020

ABSTRACT

The flux-weighted gravity-luminosity relation (FWGLR) is investigated for a sample of 477 classical Cepheids (CCs), including stars that have been classified in the literature as such but are probably not. The luminosities are taken from the literature, based on the fitting of the spectral energy distributions (SEDs) assuming a certain distance and reddening. The flux-weighted gravity (FWG) is taken from gravity and effective temperature determinations in the literature based on high-resolution spectroscopy. There is a very good agreement between the theoretically predicted and observed FWG versus pulsation period relation that could serve in estimating the FWG (and $\log g$) in spectroscopic studies with a precision of 0.1 dex. As was known in the literature, the theoretically predicted FWGLR relation for CCs is very tight and is not very sensitive to metallicity (at least for LMC and solar values), rotation rate, and crossing of the instability strip. The observed relation has a slightly different slope and shows more scatter (0.54 dex). This is due both to uncertainties in the distances and to the pulsation phase averaged FWG values. Data from future *Gaia* data releases should reduce these errors, and then the FWGLR could serve as a powerful tool in Cepheid studies.

Key words. Stars: distances - Stars: fundamental parameters - Stars: variables: Cepheids - distance scale

1. Introduction

Classical Cepheids (CCs) are considered an important standard candle because they are bright, and thus they comprise a link between the distance scale in the nearby universe and that further out via those galaxies that contain both Cepheids and SNIa (see Riess et al. 2019 for a determination of the Hubble constant to 1.9% precision, taking into account the new 1.1% precise distance to the Large Magellanic Cloud from Pietrzyński et al. 2019).

This is the third paper in a series on Galactic CCs based on the *Gaia* second data release (GDR2, *Gaia* Collaboration et al. 2018). Groenewegen (2018) (hereafter G18) started from an initial sample of 452 Galactic CCs with accurate [Fe/H] abundances from spectroscopic analysis. Based on parallax data from *Gaia* DR2, supplemented with accurate non-*Gaia* parallax data when available, a final sample of about 200 FU mode Cepheids with good astrometric solutions was retained to derive period-luminosity (*PL*) and period-luminosity-metallicity (*PLZ*) relations. The influence of a parallax zeropoint offset on the derived *PL(Z)* relation is large and means that the current GDR2 results do not allow to improve on the existing calibration of the relation or on the distance to the LMC (as also concluded by Riess et al. 2018). The zeropoint, the slope of the period dependence, and the metallicity dependence of the *PL(Z)* relations are correlated with any assumed parallax zeropoint offset.

Send offprint requests to: Martin Groenewegen

* Table A.3 is available in electronic form at the CDS via anonymous ftp to cdsarc.u-strasbg.fr (130.79.128.5) or via <http://cdsweb.u-strasbg.fr/cgi-bin/qcat?J/A+A/>. Tables A.1 and A.2, and Figure A.2 are available in the online edition of A&A.

In Groenewegen (2020) (hereafter G20) the sample was expanded to 477 stars. Using photometry over the widest available range in wavelength (and at mean light when available) the spectral energy distributions (SEDs) were constructed and fitted with model atmospheres (and a dust component when required). For an adopted distance and reddening these fits resulted in a best-fitting bolometric luminosity (*L*) and the photometrically derived effective temperature (T_{eff}). This allowed for the derivation of period-radius (*PR*) and *PL* relations, the construction of the Hertzsprung-Russell diagram (HRD), and a comparison to theoretical instability strips (ISs). The position of most stars in the HRD was consistent with theoretical predictions. Outliers were often associated with sources where the spectroscopically and photometrically determined effective temperatures differed, or with sources with large and uncertain reddenings.

In this paper the relation between bolometric absolute magnitude and the flux-weighted gravity (FWG), $g_F \sim g/T_{\text{eff}}^4$, is investigated: the so-called flux-weighted gravity-luminosity relation (FWGLR). The tight correlation between g_F and luminosity was first demonstrated by Kudritzki et al. (2003, 2008) for blue supergiants, and was then used for extragalactic distance determinations in Kudritzki et al. (2016). Anderson et al. (2016) demonstrated that theoretical pulsation models for CCs also followed a tight FWGLR, in fact tighter than the *PL* relation, and that there was a good correspondence between observed g_F and period for a sample of CCs. The latest calibration of the FWGLR is presented in Kudritzki et al. (2020) based on 445 stars ranging from $M_{\text{bol}} = +9.0$ to -8.0 .

The paper is structured as follows. In Section 2 the theoretical models of Anderson et al. (2016) are compared to the latest calibration in Kudritzki et al. (2020). In Section 3 the sample of 477 (candidate) CCs is introduced and the g_F are derived, and

the correlation with period and luminosity are presented. A brief discussion and summary concludes the paper.

2. Theoretical FWGLR for CCs

The FWG is defined as $\log g_F = \log g - 4 \cdot \log(T_{\text{eff}}/10^4)$ (Kudritzki et al. 2003). Kudritzki et al. (2020) present the latest calibration of the FWG against absolute bolometric magnitude as

$$M_{\text{bol}} = (3.19 \pm 0.01)(\log g_F - g_F^{\odot}) + (4.74 \pm 0.01) \quad (1)$$

for $\log g_F \geq \log g_F^b$ and

$$M_{\text{bol}} = (3.76 \pm 0.11)(\log g_F - g_F^b) + (-2.98 \pm 0.09) \quad (2)$$

for $\log g_F < \log g_F^b$, with a scatter of 0.17 and 0.29 mag, respectively. The break in the relation is set at $g_F^b = 3.0$, while the FWG of the Sun is $g_F^{\odot} = 5.39$.

Anderson et al. (2016) presented a large set of pulsation models for CCs based on stellar evolutionary models for a range of initial masses (1.7-15 M_{\odot}), initial rotation rates ($\omega_{\text{ini}} = 0.0, 0.5, 0.9$ in terms of the critical rotation rates), metallicities ($Z = 0.002, 0.006, 0.014$), and for fundamental mode (FU) and first overtone (FO) CCs. Stellar parameters (L, T_{eff}), and pulsation periods are given at the entry and exit of the IS for various crossings. They used these models to show the tight FWGLR for CCs for the first time (Fig. 16 in Anderson et al. 2016).

The top panel in Fig. 1 shows the theoretical FWGLR based on these models for FU pulsators with periods > 0.6 d, FO pulsators with periods > 0.4 d, $Z = 0.006$ and 0.014 , and all rotation rates and crossings of the IS as the coloured lines and symbols. Also shown are Eqs. 1 and 2. For the lower gravities the models deviate from Eq. 2, and appear to be closer to an extension of Eq. 1. A linear fit to these models gives the relation

$$M_{\text{bol}} = (3.35 \pm 0.02)(\log g_F - g_F^b) + (-2.975 \pm 0.012) \quad (3)$$

with an rms of 0.16 mag, shown as the green line in the figure. Additional fits are given in Appendix A.

The bottom panel shows the relation between FWG and period for the same selection of models (cf. Figure 17 in Anderson et al. (2016, 2020)). Periods of FO models are fundamentalised using the relation $P_0 = P_1/(0.716 - 0.027 \log P_1)$ following Feast & Catchpole (1997). The best fit is

$$\log g_F = (-0.834 \pm 0.011) \log P_0 + (3.402 \pm 0.011) \quad (4)$$

with an rms of 0.09 dex. Eliminating the second crossing models would result in a fit with a smaller scatter, but as this information is not known a priori the relation as presented is more generally applicable when an estimate of $\log g_F$ is desired. Figures and relations for FU and FO models separately are presented in the Appendix.

3. Sample and observed FWGs.

The sample studied here is the collection of 477 stars considered in G20. It is based on the original sample of 452 stars compiled in G18, extended by 25 additional stars for which accurate iron abundances have since become available, including five CCs in the inner disk of our Galaxy (Inno et al. 2019).

G20 constructed the SEDs for these stars, considering photometry from the ultraviolet to the far-infrared, and as much as possible at mean light. Distances and reddening were collected

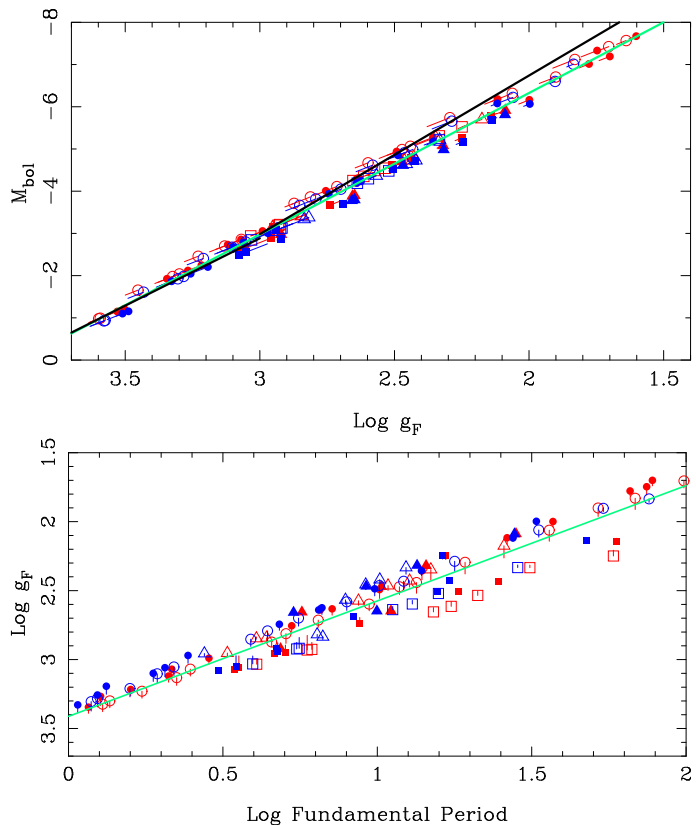


Fig. 1. *Top panel.* FWGLR based on the pulsation models in Anderson et al. (2016). FU models are shown in red, FO models are shown in blue. For clarity FU (FO) models are plotted with an offset of +0.05 (−0.05) dex in M_{bol} . Symbols indicate the entry point of the IS, the lines connect it to the exit point of the IS. The first, second, and third crossing models are plotted as circles, squares, and triangles, respectively. Solar metallicity models are plotted with open symbols, models with $Z = 0.006$ with filled symbols. The black lines refer to Eqs. 1 and 2, the green line to the best fit (Eq. 3). *Bottom panel.* Relation between FWG and period for the same models. The period of the FO models was fundamentalised. The green line refers to the best fit, Eq. 4.

from the literature. Distances from GDR2 data was available for 232 sources, and from other parallax data for 26 stars.

Luck (2018) (hereafter L18) published a list of abundances and stellar parameters for 435 Cepheids based on the analysis of 1137 spectra. L18 reduced all data in a uniform way using MARCS LTE model atmospheres (Gustafsson et al. 2008). Effective temperatures were determined in that paper using the line depth ratio (LDR) – effective temperature calibration of Kovtyukh (2007) as updated by Kovtyukh (2010, private communication to Luck), while gravities were determined from the ionisation balance between Fe I and Fe II lines, and microturbulent velocities (v_t) by forcing there to be no dependence in the per-line Fe I abundances on equivalent width (see L18 for additional details).

Table 1 contains information on the set of 52 CCs for which five or more spectra were available in L18 taken at different phases in the pulsation cycle. FWGs are calculated on the one hand from the mean effective temperatures and mean gravities (as given by L18 in his Table 11), and on the other hand from an analysis of the FWGs calculated for the individual epochs and plotted versus phase. Using the code PERIOD04 (Lenz & Breger 2005) to fit a low-order harmonic, this gives the mean $\log g_F$, the

amplitude of the $\log g_F$ curve, and the rms value. Some $\log g_F$ phased curves with fits are shown in Fig. 2.

These curves show considerable scatter even when the pulsation cycle is well sampled. This is likely due to the error bar in an individual determination of g_F . The error on effective temperature generally has a negligible contribution in this. Ninety-five percent of individual effective temperature error bars among the 1137 spectra in L18 are between 30 and 220 K with a median of 65 K. An error of 100 K at $T_{\text{eff}} = 6000$ K introduces an error of 0.03 dex in g_F , much smaller than the error on $\log g$, which was estimated to be ~ 0.15 dex by L18. A comparison of $\log g_F$ values determined from the averages of the effective temperatures and gravities, and from fitting the $\log g_F$ curve with phase show essentially the same result, especially when seven or more spectra are averaged (with an average difference between Cols. 6 and 8 of -0.02 ± 0.04 dex).

Figure 3 shows the FWGLR for the sample of 52 stars from Table 1, where the luminosity and error are taken from G20. Equations 1, 2, and 3 are plotted as reference. Using a linear bi-sector fit (using the code SIXLIN from Isobe et al. 1990) the best fit is

$$M_{\text{bol}} = (2.79 \pm 0.18)(\log g_F - 2.5) + (-4.21 \pm 0.08) \quad (5)$$

with an rms of 0.38 mag (blue line in the figure). A standard least-squares fit has a shallower slope of 2.54. The theoretical fit is shown in Eq. 3, and this fit differs by about 0.4 mag at $\log g_F = 2.5$. Alternatively, the observed $\log g_F$ values are systematically too small by $0.4/2.8 \sim 0.14$ dex. At lower FWG or longer periods the difference with the theoretical relation is larger.

Table A.3 collects the FWG data for the entire sample of 477 stars. Overall, most of the data (435 stars) come from L18, and for the remaining stars $\log g$ and T_{eff} have been collected from the literature in order to calculate $\log g_F$. Multiple determinations of $\log g_F$ have been averaged and so can differ slightly from the values in Table 1. The table also includes the period, pulsation type, distance with error, and luminosity with error from G20. Figure 4 shows the observational equivalent to the bottom panel in Fig. 1, the FWG determined from spectroscopy against pulsation period (fundamentalised for FO pulsators).

There is a tight correlation between the two quantities. Removing non-CCs (see Table A.3) and applying iterative 3σ clipping results in the fit

$$\log g_F = (-0.80 \pm 0.03) \log P_0 + (3.43 \pm 0.03) \quad (6)$$

with an rms of 0.16 dex, in very good agreement with the theoretically predicted relation. Interestingly, many of the outliers come from a single source, Genovali et al. (2014), who derived very low $\log g$ values for some objects. Some additional information and fits are provided in Appendix A.

Figure 5 is the equivalent to Fig. 3 for the entire sample, using a simple averaging of the available FWGs. The error on distance is now taken into account in calculating the error on luminosity. Following the discussion above and in the Appendix, the data from Genovali et al. (2014) has been excluded, and to reduce the scatter only stars with two or more spectra are considered. A linear bi-sector fit applying iterative 3σ clipping results in

$$M_{\text{bol}} = (2.93 \pm 0.13)(\log g_F - 2.5) + (-4.23 \pm 0.06) \quad (7)$$

with an rms of 0.54 mag using 170 stars and is shown as the blue line in the figure. This is currently the best observational determination of the FWGL relation for CCs.

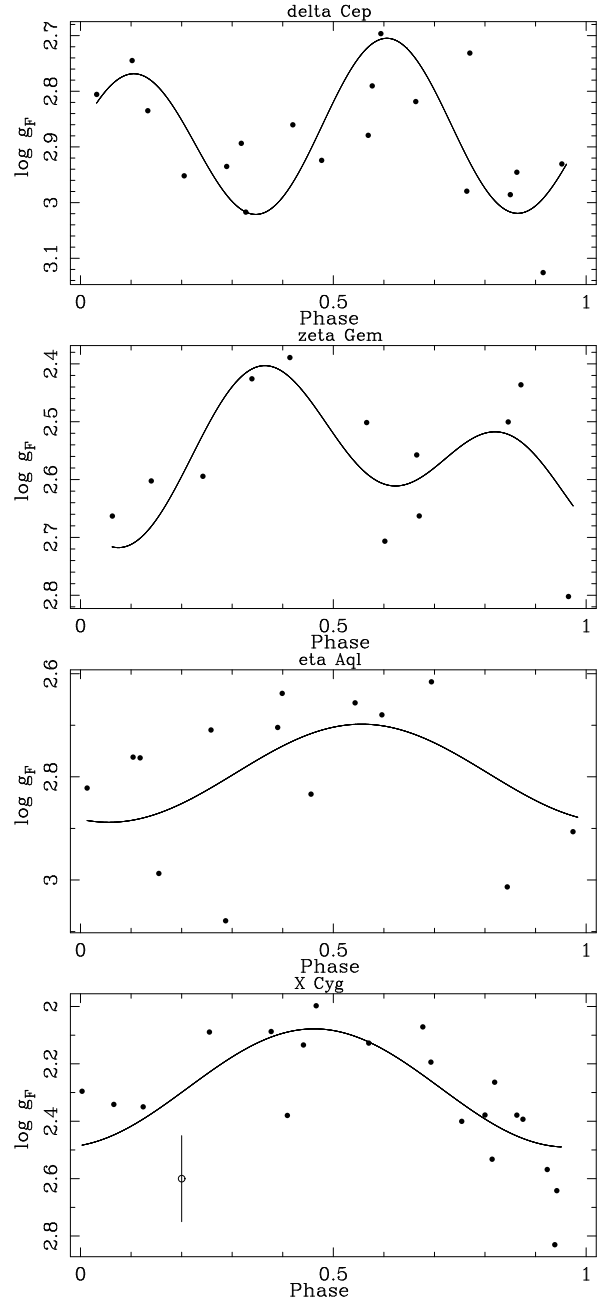


Fig. 2. FWG vs pulsation phase for four CCs. The typical error bar in each point is 0.15 dex in FWG, as indicated in the bottom plot. The lines are low-order harmonic fits to the data (see Col. 7 in Table 1).

4. Discussion and summary

The relation between FWG and period, and FWG and bolometric luminosity is investigated for a sample 477 CCs. The FWGs are derived from effective temperatures and $\log g$ values available in the literature based on high-resolution spectroscopy. The overall majority of parameters have been compiled from a single source (L18) that determined $\log g$ and T_{eff} in an uniform manner. For a subset of stars multiple-phase data is available. The FWG-Period and FWGLR are compared to theoretical models from Anderson et al. (2016)

A very good agreement is found between the theoretical and observed relations between FWG and period. These relations could serve as a prediction for a reasonable range in $\log g$ values (assuming an effective temperature) in a spectroscopic analysis.

Table 1. FWGL data for the subsample with more than five spectra.

Name	Period (days)	N_{spec}	$\langle T_{\text{eff}} \rangle$ (K)	$\langle \log g \rangle$ (cgs)	$\langle \log g_{\text{F}} \rangle$ (cgs)	N_{h}	$\log g_{\text{F}}$ (cgs)	Ampl (cgs)	rms (cgs)	Luminosity (L_{\odot})
V473 Lyr	1.490780	5	6019	2.30	3.18	1	3.205	0.056	0.006	572.3 ± 10.8
SU Cas	1.949324	13	6274	2.26	3.07	2	3.065	0.122	0.046	1027.0 ± 16.6
DT Cyg	2.499215	14	6192	2.27	3.10	1	3.108	0.049	0.066	157.6 ± 70.7
SZ Tau	3.148730	16	5987	2.03	2.92	1	2.937	0.079	0.081	1155.3 ± 23.1
V1334 Cyg	3.332816	11	6293	2.22	3.02	1	3.014	0.119	0.082	1879.5 ± 384.2
RT Aur	3.728485	12	5948	2.06	2.96	1	2.978	0.048	0.031	970.8 ± 46.1
SU Cyg	3.845547	12	6036	2.08	2.96	1	2.988	0.067	0.136	909.6 ± 294.7
ST Tau	4.034299	7	6052	2.07	2.94	1	2.910	0.078	0.059	1155.3 ± 23.1
BQ Ser	4.270900	7	6040	2.16	3.04	1	2.860	0.294	0.129	1876.3 ± 97.1
Y Lac	4.323776	10	5915	1.87	2.78	1	2.779	0.111	0.108	1250.6 ± 82.7
T Vul	4.435462	12	5852	2.03	2.96	1	2.949	0.131	0.109	691.9 ± 27.6
FF Aql	4.470881	14	6164	2.04	2.88	1	2.886	0.085	0.086	2237.6 ± 118.3
CF Cas	4.875220	7	5672	1.74	2.73	1	2.748	0.129	0.142	1284.7 ± 41.1
BG Lac	5.331908	9	5674	1.70	2.68	2	2.710	0.218	0.035	1303.6 ± 43.2
delta Cep	5.366341	19	5854	1.96	2.89	3	2.878	0.108	0.068	1984.8 ± 587.1
Y Sgr	5.773350	12	5767	1.77	2.73	1	2.724	0.088	0.096	1737.4 ± 90.1
FM Aql	6.114290	12	5766	1.68	2.64	1	2.667	0.085	0.128	2575.5 ± 91.8
X Vul	6.319588	8	5753	1.81	2.77	1	2.774	0.074	0.113	1735.3 ± 81.7
XX Sgr	6.424140	5	5805	1.81	2.75	1	2.671	0.126	0.032	1913.5 ± 123.3
AW Per	6.463589	11	5928	1.86	2.77	2	2.776	0.153	0.079	1646.8 ± 76.6
U Sgr	6.745226	11	5709	1.79	2.76	2	2.769	0.178	0.086	2421.8 ± 69.6
U Aql	7.024049	5	5565	1.64	2.66	1	2.654	0.077	0.026	1619.1 ± 42.2
eta Aql	7.176915	14	5746	1.86	2.82	1	2.793	0.095	0.124	3008.4 ± 598.2
BB Her	7.507945	8	5641	1.65	2.64	1	2.655	0.075	0.091	3122.0 ± 153.2
RS Ori	7.566881	7	5891	1.77	2.69	1	2.693	0.109	0.112	2683.4 ± 85.8
V440 Per	7.570000	10	6056	1.97	2.84	1	2.829	0.087	0.109	3257.4 ± 50.3
W Sgr	7.595030	9	5765	1.78	2.74	1	2.726	0.096	0.126	3277.6 ± 312.9
RX Cam	7.912024	10	5703	1.65	2.63	1	2.642	0.166	0.087	2192.7 ± 87.0
W Gem	7.913779	13	5771	1.69	2.64	1	2.662	0.131	0.074	3631.9 ± 179.0
U Vul	7.990676	8	5779	1.73	2.68	1	2.673	0.042	0.069	5408.2 ± 241.2
DL Cas	8.000669	11	5682	1.56	2.54	2	2.566	0.189	0.049	1957.5 ± 49.4
V636 Cas	8.375710	8	5505	1.47	2.51	1	2.508	0.036	0.038	3268.0 ± 81.6
S Sge	8.382086	11	5689	1.73	2.71	1	2.743	0.133	0.098	2286.1 ± 57.8
V500 Sco	9.316863	5	5675	1.56	2.54	1	2.543	0.042	0.062	2654.7 ± 143.3
FN Aql	9.481640	11	5488	1.38	2.42	1	2.456	0.181	0.106	2699.4 ± 68.5
YZ Sgr	9.553606	11	5653	1.69	2.68	1	2.681	0.026	0.074	3438.5 ± 126.8
zeta Gem	10.150730	12	5512	1.52	2.55	2	2.562	0.126	0.080	3203.4 ± 928.2
Z Lac	10.885613	10	5618	1.49	2.49	2	2.499	0.119	0.058	4173.7 ± 193.5
VX Per	10.889040	12	5783	1.64	2.59	1	2.579	0.130	0.147	4407.1 ± 107.4
RX Aur	11.626000	13	5782	1.67	2.62	1	2.623	0.155	0.085	4670.0 ± 204.7
TT Aql	13.754912	10	5272	1.15	2.26	2	2.400	0.402	0.104	5242.1 ± 206.0
SV Mon	15.232780	9	5330	1.11	2.20	1	2.220	0.237	0.136	4952.3 ± 352.7
X Cyg	16.386332	20	5252	1.10	2.22	1	2.284	0.206	0.140	5201.9 ± 280.9
RW Cam	16.415014	17	5213	1.03	2.16	1	2.200	0.100	0.156	4857.7 ± 187.4
CD Cyg	17.073967	17	5394	1.19	2.26	2	2.230	0.270	0.103	5399.7 ± 191.6
Y Oph	17.124130	14	5819	1.62	2.56	1	2.561	0.088	0.061	12857.9 ± 388.4
SZ Aql	17.141247	11	5398	1.20	2.27	2	2.299	0.150	0.084	7077.7 ± 232.3
WZ Sgr	21.849709	10	5140	0.88	2.04	2	2.204	0.514	0.060	8349.1 ± 239.9
X Pup	25.961000	8	5353	0.75	1.84	1	1.923	0.374	0.073	9419.5 ± 552.9
T Mon	27.024649	12	5108	0.93	2.10	1	2.115	0.162	0.141	8163.2 ± 203.3
SV Vul	45.012100	15	5329	0.85	1.94	1	1.905	0.124	0.157	27925.1 ± 1818.3
S Vul	68.463997	6	5452	0.93	1.98	1	1.929	0.281	0.082	21197.2 ± 747.9

Notes. Column 1: Name. Column 2: Period (as quoted in L18). Column 3: Number of spectra L18. Column 4: Average effective temperature (quoted in Table 11 in L18). Column 5: Average $\log g$ (quoted in Table 11 in L18). Column 6: Average $\log g_{\text{F}}$ based on Cols. 4 and 5. Column 7: Number of harmonics used in the time analysis. Column 8: Mean $\log g_{\text{F}}$. Column 9: Amplitude in the $\log g_{\text{F}}$ curve. Column 10: RMS. Column 11: Luminosity and error (from Table 1 in G20). The error is the fit error, and does not include the error on the distance. The distance and error on the distance needed to calculate the total error on L are given in Table A.3.

The observed FWGLR is found to have a shallower slope than the theoretical relation. It is not clear at the moment if this is a significant effect or not. As the observed relation between FWG and period agrees with the theoretical relation, one would be inclined to think that there could be a systematic effect in the bolometric magnitudes of the long-period Cepheids. They are

rarer and on average at longer distance, likely to be more susceptible to (systematic) errors on parallax. This is qualitatively confirmed by repeating the fit of Eq. 7 restricting the sample to stars with $\sigma_{\text{L}}/L < 0.2$. The slope is increased, but has a larger error bar (3.05 ± 0.19) and the rms is reduced to 0.44 mag.

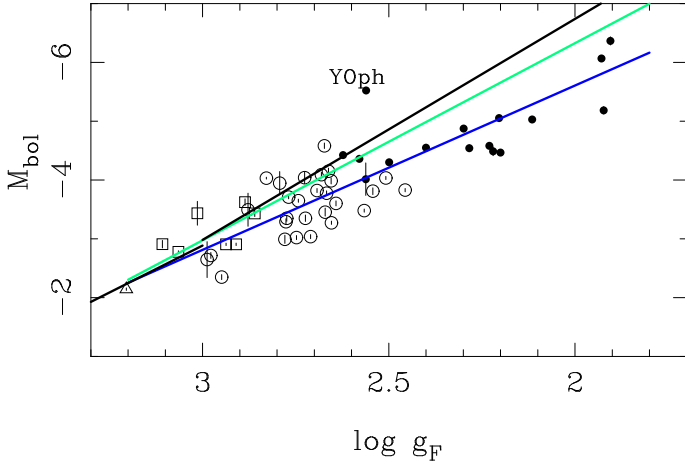


Fig. 3. FWGLR based on the subsample with more than five spectra. FU mode pulsators are plotted as circles (filled circles for periods over 10 days), FO pulsators as open squares, the single second-overtone pulsator as open triangle. The black lines refer to Eqs. 1 and 2, the green line to Eq. 3. The blue line is a fit to the data points, excluding Y Oph (Eq. 5).

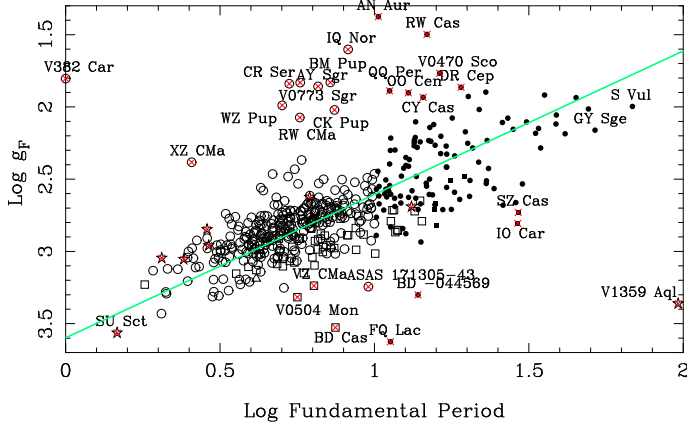


Fig. 4. FWG vs fundamental pulsation period. Some outliers are named. The green line refers to the best fit, Eq. 7, which excludes the outliers and non-CCs indicated by a red cross.

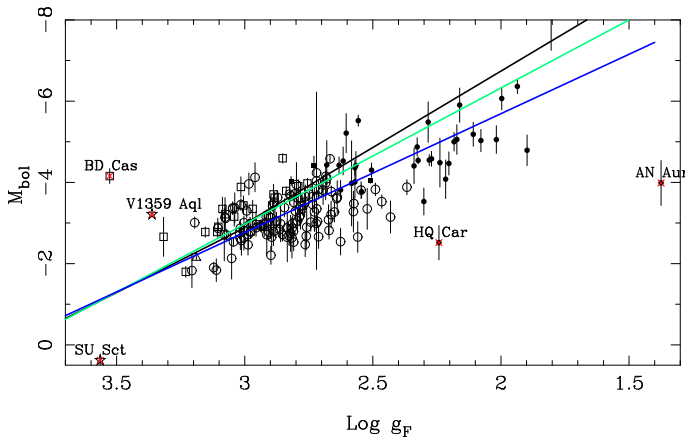


Fig. 5. FWGLR, with some outliers named. The black lines refer to Eqs. 1 and 2, the green line to Eq. 3. The blue line refers to the best fit, Eq. 7, which excludes the outliers and non-CCs indicated by a red cross. Outliers located outside the plot window are SU Cru ($\log g_F = 0.19$, $M_{\text{bol}} = -3.7$), SY Nor ($\log g_F = 2.4$, $M_{\text{bol}} = +3.3$), and V382 Car ($\log g_F = 1.8$, $M_{\text{bol}} = -8.6$).

On the other hand, although the T_{eff} determinations based on the LDR method are precise (as discussed earlier), possible systematic effects (which would also affect the determination of $\log g$ and $\log g_F$) could play a role (Mancino et al. 2020). For the subsample of 52 stars in L18 with five or more spectra, the cycle averaged T_{eff} s (as quoted in Table 1) are compared to the photometrically derived T_{eff} s based on the SED fitting in G20. The errors on the photometrically derived effective temperatures (the median is 180 K) are larger than those derived from spectroscopy. There are two outliers Y Oph and S Vul, where the photometrically derived temperatures are considerably lower than those quoted in L18 (570 and 830 K; $> 4.3 \sigma$). For the other stars the difference (spectroscopically - photometrically derived T_{eff}) is 140 ± 150 K.

Systematic errors on the determination of the gravity could also play a role. The methodology used by L18 to determine the stellar parameters, in particular ν_t and gravity, is the standard one. A non-standard method is sometimes also used in the literature, as introduced by Kovtyukh & Andrievsky (1999). To avoid non-LTE-sensitive stronger Fe I lines, ν_t is derived from Fe II lines and weak Fe I lines alone. This leads to higher ν_t , which in turn leads to higher gravities when the ionisation balance is enforced. For δ Cep Kovtyukh & Andrievsky (1999) find that the gravities are higher by 0.5 dex using the non-standard method. The matter is also debated in Yong et al. (2006). They note that the non-standard method ‘has merits’, but show that their derived gravities using the standard method are self-consistent, one argument being that this gravity also produces ionisation equilibrium for Ti I lines that are more susceptible to non-LTE effects than Fe. The non-standard method is also used in Takeda et al. (2013). Anderson et al. (2016) excluded the gravities from that paper as they differed from other sources they used. Twelve stars overlap with the sample of stars with multi-epoch data from L18 (in Table 1). Takeda et al. (2013) present stellar parameters at between 7 and 17 epochs. The mean effective temperatures and mean gravities are calculated, as well are FWGs at these epochs based on the data in Takeda et al. (2013), and fitted with low-order harmonic sine curves, as before, to give the mean FWG. The difference (min - max (mean)) between the parameters from the non-standard method minus those from the standard method are $-8 - +444$ (167) K in T_{eff} , $+0.22 - +0.72$ (+0.36) dex in $\log g$, and $+0.11 - +0.67$ (+0.34) dex in FWG, with tendencies that the difference in all three quantities decreases with increasing period.

The FWGLR has the potential to be an alternative to the PL relation in distance determination (Anderson et al. 2016). In its current empirically best calibrated version it is not. The scatter of 0.54 mag is larger than the 0.40 mag in the bolometric PL relation determined in G20 using the identical sample of stars, distances, and luminosities.

One issue is that the independent variable period is known with great precision, while the independent variable FWG has a non-negligible error associated with it. The fitting of the FWG versus pulsation phase did not provide more precise mean FWGs than simple averaging. As the slope of the FWGLR is reasonably steep, any uncertainty on the FWG leads to a three times larger uncertainty in M_{bol} .

The discussion above also demonstrates that the stellar parameters should be derived in a uniform way. To exclude the influence of data analysis inhomogeneity altogether, Eq. 7 was re-determined using data only from L18. The usable sample is reduced to 161 stars and the slope and offset change marginally, less than 1σ . The standard approach used by L18 seems to give consistent results when considering the compari-

son to theory and the independent calibration of the FWGLR by Kudritzki et al. (2020). Changes in the FWG by $\sim +0.3-0.5$ dex, as implied by the non-standard method, would result in a disagreement.

This paper is written with the tremendous potential offered by *Gaia* in mind. Future data releases will provide information that will impact and improve on the results obtained here. Primarily, improved parallaxes, taking into account binarity in the astrometrical solution, will provide more precise distances and thus bolometric luminosities (e.g. through the SED fitting performed in G20).

Secondly, *Gaia* RVS spectra and *Gaia* Bp/Rp spectrophotometry will provide estimates of the stellar parameters ($\log g$, T_{eff} , also metallicity) in future releases. Only mean spectra in data release 3, and epoch spectra in data release 4 (Brown 2019). An older analysis by Recio-Blanco et al. (2016) indicate that end-of-mission accuracies in $\log g$ of 0.1 dex or better can be reached in intermediate-metallicity F and G giants of magnitude $G \sim 10.3 - 11.8$ or brighter. Spectro-photometry can go fainter but with poorer accuracies (0.2-0.4 dex in $\log g$ down to $G = 19$; Table 4 in Bailer-Jones et al. 2013). As the nominal mission of 5 years is extended, by +18 months until the end of 2020, and likely until the end of 2022, these numbers should improve. In conclusion, the FWGLR could prove to become an extremely useful tool in Cepheid studies.

Acknowledgements. I would like to thank Dr. Bertrand Lemasle for interesting discussion on the determination of $\log g$ and commenting on a draft version of this paper. This research has made use of the SIMBAD database and the VizieR catalogue access tool operated at CDS, Strasbourg, France.

References

- Anders, F., Khalatyan, A., Chiappini, C., et al. 2019, A&A, 628, A94
 Anderson, R. I., Saio, H., Ekström, S., Georgy, C., & Meynet, G. 2016, A&A, 591, A8
 Anderson, R. I., Saio, H., Ekström, S., Georgy, C., & Meynet, G. 2020, A&A, 638, C1
 Andrievsky, S. M., Kovtyukh, V. V., Luck, R. E., et al. 2002a, A&A, 381, 32
 Andrievsky, S. M., Kovtyukh, V. V., Luck, R. E., et al. 2002b, A&A, 392, 491
 Andrievsky, S. M., Kovtyukh, V. V., & Usenko, I. A. 1994, A&A, 281, 465
 Andrievsky, S. M., Lépine, J. R. D., Korotin, S. A., et al. 2013, MNRAS, 428, 3252
 Andrievsky, S. M., Luck, R. E., Martin, P., & Lépine, J. R. D. 2004, A&A, 413, 159
 Andrievsky, S. M., Martin, P., Kovtyukh, V. V., Korotin, S. A., & Lépine, J. R. D. 2016, MNRAS, 461, 4256
 Bailer-Jones, C. A. L., Andrae, R., Arcay, B., et al. 2013, A&A, 559, A74
 Boyarchuk, A. A. & Lyubimkov, L. S. 1981, Bulletin Crimean Astrophysical Observatory, 64, 1
 Brown, A. G. A. 2019, in The Gaia Universe, 18
 Feast, M. W. & Catchpole, R. M. 1997, MNRAS, 286, L1
 Gaia Collaboration, Brown, A. G. A., Vallenari, A., et al. 2018, A&A, 616, A1
 Genovali, K., Lemasle, B., Bono, G., et al. 2014, A&A, 566, A37
 Groenewegen, M. A. T. 2018, A&A, 619, A8
 Groenewegen, M. A. T. 2020, A&A, 635, A33
 Gustafsson, B., Edvardsson, B., Eriksson, K., et al. 2008, A&A, 486, 951
 Inno, L., Urbaneja, M. A., Matsunaga, N., et al. 2019, MNRAS, 482, 83
 Isobe, T., Feigelson, E. D., Akritas, M. G., & Babu, G. J. 1990, ApJ, 364, 104
 Kovtyukh, V. V. 2007, MNRAS, 378, 617
 Kovtyukh, V. V. & Andrievsky, S. M. 1999, A&A, 351, 597
 Kovtyukh, V. V., Wallerstein, G., & Andrievsky, S. M. 2005, PASP, 117, 1173
 Kudritzki, R. P., Bresolin, F., & Przybilla, N. 2003, ApJ, 582, L83
 Kudritzki, R. P., Castro, N., Urbaneja, M. A., et al. 2016, ApJ, 829, 70
 Kudritzki, R.-P., Urbaneja, M. A., Bresolin, F., et al. 2008, ApJ, 681, 269
 Kudritzki, R.-P., Urbaneja, M. A., & Rix, H.-W. 2020, ApJ, 890, 28
 Lemasle, B., François, P., Bono, G., et al. 2007, A&A, 467, 283
 Lemasle, B., François, P., Piersimoni, A., et al. 2008, A&A, 490, 613
 Lemasle, B., Kovtyukh, V., Bono, G., et al. 2015, A&A, 579, A47
 Lenz, P. & Breger, M. 2005, Communications in Asteroseismology, 146, 53
 Luck, R. E. 2018, AJ, 156, 171
 Luck, R. E., Gieren, W. P., Andrievsky, S. M., et al. 2003, A&A, 401, 939
 Luck, R. E., Kovtyukh, V. V., & Andrievsky, S. M. 2006, AJ, 132, 902
 Mancino, S., Romaniello, M., Anderson, R. I., & Kudritzki, R.-P. 2020, arXiv e-prints, arXiv:2001.05881
 Martin, R. P., Andrievsky, S. M., Kovtyukh, V. V., et al. 2015, MNRAS, 449, 4071
 Pietrzyński, G., Graczyk, D., Gallette, A., et al. 2019, Nature, 567, 200
 Recio-Blanco, A., de Laverny, P., Allende Prieto, C., et al. 2016, A&A, 585, A93
 Riess, A. G., Casertano, S., Yuan, W., et al. 2018, ApJ, 861, 126
 Riess, A. G., Casertano, S., Yuan, W., Macri, L. M., & Scolnic, D. 2019, ApJ, 876, 85
 Romaniello, M., Primas, F., Mottini, M., et al. 2008, A&A, 488, 731
 Schmidt, E. G., Rogalla, D., & Thacker-Lynn, L. 2011, AJ, 141, 53
 Takeda, Y., Kang, D. I., Han, I., Lee, B. C., & Kim, K. M. 2013, MNRAS, 432, 769
 Watson, C. L., Henden, A. A., & Price, A. 2006, Society for Astronomical Sciences Annual Symposium, 25, 47
 Yong, D., Carney, B. W., Teixeira de Almeida, M. L., & Pohl, B. L. 2006, AJ, 131, 2256

Appendix A: Additional material

Additional fits for the FWGLR based on the models of Anderson et al. (2016) are given in Table A.1 for the three different metallicities, and with the slope fixed to the value in Eq. 3. The results for $Z = 0.006$ and 0.014 agree within the error and justify the use of a single relation combining the two metallicities (Eq. 3). The $Z = 0.002$ models differ by a larger amount, qualitatively in agreement with the remark in Kudritzki et al. (2020) on the fact that low metallicities (below -0.6 dex) have an effect on the FWGLR.

Table A.1. Fits of the type $M_{\text{bol}} = a \cdot (\log g - g_F^b) + b$.

a	b	rms	metallicity
3.381 ± 0.025	-3.031 ± 0.014	0.13	$Z = 0.014$
3.35 fixed	-3.040 ± 0.014	0.14	
3.331 ± 0.029	-2.912 ± 0.017	0.16	$Z = 0.006$
3.35 fixed	-2.905 ± 0.014	0.16	
3.426 ± 0.026	-2.732 ± 0.016	0.17	$Z = 0.002$
3.35 fixed	-2.759 ± 0.012	0.18	

The bottom panel of Fig. 1 and Eq. 4 present the relation between FWG and pulsation period based on the models of Anderson et al. (2016) with the overtone periods converted to FU periods. Figure A.1 and Eqs. A.1 and A.2 give the results for FU and FO pulsators separately. The best fits are

$$\log g_F = (-0.847 \pm 0.015) \log P + (3.431 \pm 0.016) \quad (\text{A.1})$$

with an rms of 0.10 dex for the FU models, and

$$\log g_F = (-0.840 \pm 0.016) \log P + (3.255 \pm 0.013) \quad (\text{A.2})$$

with an rms of 0.08 dex for the FO models.

Additional fits for the relations between FWG and period are given in Table A.2 and are illustrated in Fig. A.2. They show that when multiple g_F values are available the scatter in the relation decreases. Assuming that the intrinsic scatter in the relation is 0.093 dex (Eq. 4) a single determination has an estimated error of about 0.13 dex (dominated by the error on $\log g$), while averaging six or more spectra leads to an error of about 0.09 dex.

As noted in the main text, and illustrated by comparing Fig. 4 and the top panel in Fig. A.2, a fair fraction of outliers are stars with T_{eff} and $\log g$ taken from Genovali et al. (2014). Genovali et al. (2014) also present multiple observations for some stars, and XX Sgr and WZ Sgr are in common with the subsample of stars in L18 with five or more available spectra. A comparison shows that the difference in $\log g_F$ is dominated by the difference in $\log g$, that are of the order 0.5 dex. For some of the stars in the present sample the $\log g_F$ (and $\log g$) values are too low by 1 dex. As they seem to use the same methodology as L18 in deriving the stellar parameters, no simple explanation is offered to explain this discrepancy.

Table A.3 compiles the FWG and luminosity data for the entire sample. The full table is available at the CDS.

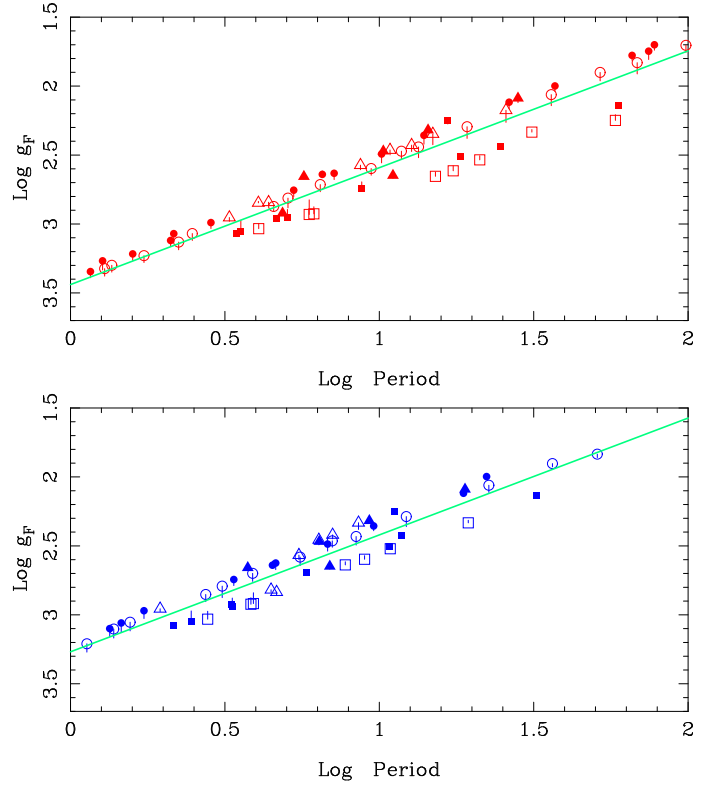


Fig. A.1. Relation between FWG and period for FU (top panel) and FO (bottom panel) models. The meaning of the symbols and colours is explained in Fig 1. The green lines refer to the best fits, Eqs. A.1 and A.2.

Table A.2. Fits of the type $g_F = a \cdot \log P + b$.

a	b	rms	N	Remarks
-0.802 ± 0.028	3.436 ± 0.025	0.159	443	standard, Eq. 7
-0.804 ± 0.028	3.438 ± 0.025	0.158	442	excluding Genovali et al. (2014)
-0.793 ± 0.036	3.438 ± 0.032	0.160	275	$N_{\text{sp}} = 1$, excluding Genovali et al. (2014)
-0.752 ± 0.073	3.381 ± 0.060	0.172	87	$N_{\text{sp}} = 2$, excluding Genovali et al. (2014)
-0.630 ± 0.116	3.351 ± 0.100	0.160	32	$N_{\text{sp}} = 3 - 5$, excluding Genovali et al. (2014)
-0.805 ± 0.106	3.370 ± 0.110	0.139	20	$N_{\text{sp}} = 6 - 10$, excluding Genovali et al. (2014)
-1.046 ± 0.088	3.663 ± 0.086	0.125	31	$N_{\text{sp}} \geq 11$, excluding Genovali et al. (2014)
-0.970 ± 0.063	3.560 ± 0.064	0.127	50	$N_{\text{sp}} \geq 6$, excluding Genovali et al. (2014)

Table A.3. FWG data for the entire sample (first entries only).

Name	Type	Period (days)	d (kpc)	σ_d (kpc)	L (L_\odot)	σ_L (L_\odot)	N_{spec}	$\log g_F$ (cgs)	$\sigma_{\log g_F}$ (cgs)	Min-Max (cgs)	Ref.
AA Gem	DCEP	11.302	3.400	0.829	3400.0	122.7	2	2.216	0.11	0.04	1
AA Mon	DCEP	3.938	3.922	0.709	922.8	33.6	1	3.211	0.16	-	1
AB Cam	DCEP	5.788	4.200	0.966	1463.5	79.3	1	2.754	0.15	-	1
AC Mon	DCEP	8.014	2.400	0.400	1991.6	42.2	4	2.766	0.08	0.21	1
AD Cam	DCEP	11.261	4.600	0.756	2048.8	87.0	2	2.301	0.11	0.07	1
AD Cru	DCEP	6.398	2.994	0.394	1881.9	93.2	1	2.730	0.15	-	1
AD Gem	DCEP	3.788	2.500	0.673	966.0	32.0	2	2.914	0.11	0.12	1
AD Pup	DCEP	13.596	4.100	0.946	4650.8	356.8	1	2.103	0.15	-	1
AE Tau	DCEP	3.897	3.367	0.606	953.2	11.9	1	2.802	0.15	-	1
AE Vel	DCEP	7.134	2.100	0.187	1842.6	169.2	1	2.663	0.15	-	1
AG Cru	DCEP	3.837	1.506	0.094	1773.5	49.7	1	2.864	0.15	-	1
AH Vel	DCEPS	4.227	0.752	0.035	2604.0	37.7	2	2.838	0.11	0.04	1
alpha UMi	DCEPS	3.970	0.133	0.002	2410.9	622.8	2	2.888	0.11	0.14	2,3
AN Aur	DCEP	10.291	3.400	0.985	3124.5	58.2	2	2.630	0.11	0.24	1
AO Aur	DCEP	6.763	3.400	0.839	1620.9	49.3	3	2.728	0.09	0.18	1
AO CMa	DCEP	5.816	3.600	0.434	1197.9	58.1	1	2.950	0.16	-	1
AP Pup	DCEP	5.084	1.183	0.051	2579.5	87.4	1	2.869	0.15	-	1
AP Sgr	DCEP	5.058	0.861	0.041	1651.8	38.7	1	2.780	0.15	-	1
AQ Car	DCEP	9.769	3.030	0.317	3837.4	289.0	1	2.702	0.15	-	1
AQ Pup	DCEP	30.149	2.900	0.336	11481.5	330.8	1	2.533	0.15	-	1
AS Per	DCEP	4.973	1.200	0.087	1042.0	36.7	2	2.810	0.11	0.30	1
AT Pup	DCEP	6.665	1.637	0.085	2495.6	194.9	1	2.757	0.15	-	1
AV Cir	DCEPS	3.065	0.944	0.033	2169.7	85.7	1	2.843	0.15	-	1
AV Sgr	DCEP	15.415	2.100	0.287	4413.1	139.5	1	2.609	0.15	-	1
AW Per	DCEP	6.464	0.700	0.044	1646.8	76.6	11	2.802	0.05	0.47	1
AX Cir	DCEP	5.273	0.500	0.151	1854.6	33.1	3	2.782	0.09	0.08	1
AX Vel	DCEP(B)	2.593	1.517	0.077	1750.2	166.6	2	3.047	0.11	0.05	1
AY Cen	DCEP	5.310	1.689	0.100	1864.4	303.0	1	2.821	0.15	-	1
AZ Cen	DCEPS	3.212	2.137	0.158	2017.4	50.1	1	2.986	0.15	-	1
BB Cen	DCEPS	3.998	3.610	0.363	3100.8	110.7	1	2.888	0.15	-	1
BB Gem	DCEP	2.308	4.082	0.825	1135.9	49.5	1	3.123	0.16	-	1
BB Her	DCEP	7.508	3.623	0.759	3122.0	153.2	8	2.684	0.05	0.32	1
BB Sgr	DCEP	6.637	0.700	0.023	1529.1	30.8	1	2.800	0.15	-	1
BC Pup	DCEP	3.544	6.500	1.109	938.2	64.4	2	2.760	0.11	0.13	4,(17)

Notes. Column 1: Name. Column 2: Type (from Table 1 in G20). Nomenclature follows that used by the VSX (Watson et al. 2006)^a. Column 3: Period (from G20). Column 4: Distance (from G20). Column 5: Error on distance (from G20). Column 6: Luminosity (from G20). Column 7: Error on Luminosity (from G20). The error is the fit error, and does not include the error on the distance. If the total error on L is desired it can be calculated from $\sqrt{\sigma_L^2 + \Delta^2}$ with $\Delta = L \cdot ((1 + \sigma_d/d)^2 - 1)$. The total error is plotted in Fig. 5. Column 8: Number of available spectra, N_{spec} . Column 9: Average of available $\log g_F$ values. Column 10: Estimated error on the average $\log g_F$ value. This includes the error on T_{eff} (when not given in the reference a conservative value of 100 K has been used) and the error on $\log g$ (assumed to be 0.15 dex, unless given specifically), divided by $\sqrt{N_{\text{spec}}}$. Column 11: Difference between highest and lowest $\log g_F$ value. Column 12: References for $\log g$ and T_{eff} values to calculate $\log g_F$ and error: (1) Luck (2018), (2) Andrievsky et al. (1994), (3) Boyarchuk & Lyubimkov (1981), (4) Luck et al. (2003), (5) Schmidt et al. (2011), (6) Andrievsky et al. (2002b), (7) Lemasle et al. (2008), (8) Andrievsky et al. (2013), (9) Kovtyukh et al. (2005), (10) Luck et al. (2006), (11) Yong et al. (2006), (12) Lemasle et al. (2015), (13) Romaniello et al. (2008), (14) Andrievsky et al. (2004), (15) Lemasle et al. (2007), (16) Andrievsky et al. (2002a), (17) Genovali et al. (2014), (18) Anders et al. (2019), (19) Martin et al. (2015), (20) Andrievsky et al. (2016), (21) Inno et al. (2019). Numbers in parentheses indicate references not considered.

^a described in <https://www.aavso.org/vsx/index.php?view=about.vartypes>.

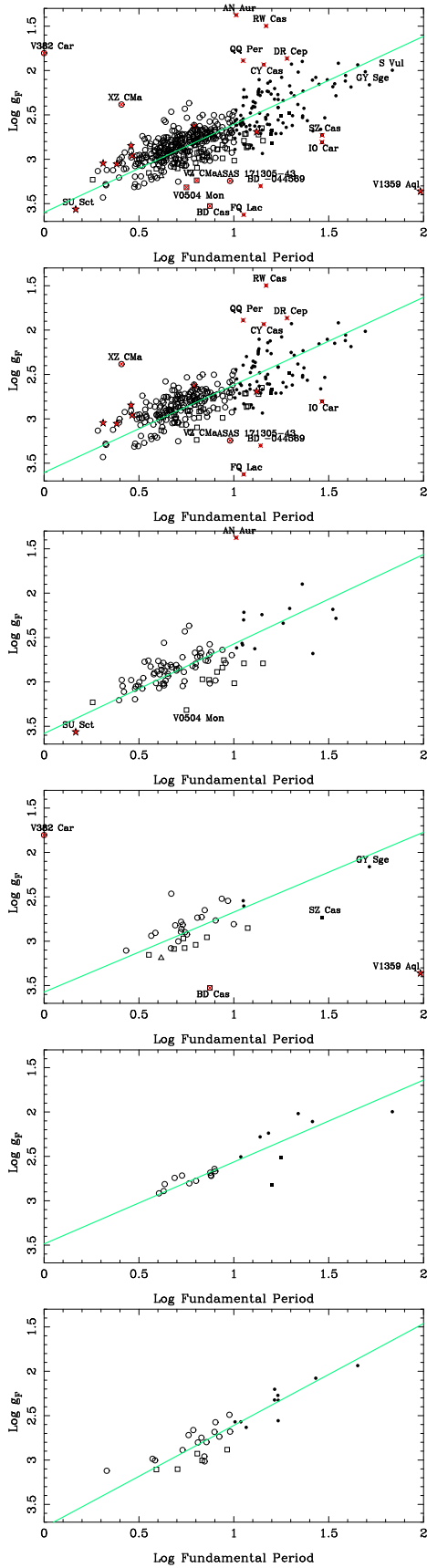


Fig. A.2. FWG vs period. The data from Genovali et al. (2014) is excluded in all plots. Different panels show different selections on the number of available g_F values. From top to bottom: all, $N_{sp} = 1$, $N_{sp} = 2$, $N_{sp} = 3 - 5$, $N_{sp} = 6 - 10$, $N_{sp} \geq 11$. The green lines refer to the best fits (see Table A.2).